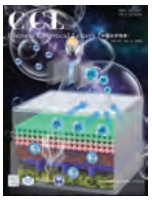
Chinese Chemical Letters 37 (2026) 110750

Contents lists available at ScienceDirect

Chinese Chemical Letters

journal homepage: www.elsevier.com/locate/cclet



Polyoxometalate-based supramolecular ionic network electrolytes for flexible proton conductors

Xiang Li, Haikun Guo, Shengchao Chai*, Haibin Li, Shihao Song, Peng Zuo, Haolong Li*

State Key Laboratory of Supramolecular Structure and Materials, College of Chemistry, Jilin University, Changchun 130012, China

ARTICLE INFO

Article history:
Received 25 October 2024
Revised 4 December 2024
Accepted 11 December 2024
Available online 12 December 2024

Keywords:
Polyoxometalate nanoclusters
Zwitterionic liquids
Supramolecular ionic networks
Proton conductors
Flexible electrolytes

ABSTRACT

Proton-conducting materials are essential for energy and electronic technologies. Polyoxometalates (POMs), as molecularly well-defined metal oxide nanoclusters with high proton conductivity, are promising candidates for such applications. However, their intrinsic crystalline brittleness poses significant challenges for practical device processing. In this work, we present a strategy to incorporate POM nanoclusters into supramolecular ionic networks (SINs). By using synergistic electrostatic and hydrogen bonding interactions, we uniformly disperse POM nanoclusters into zwitterionic liquids, forming an ionic network structure. The resulting POM-based SIN electrolytes exhibit semi-solid flexibility and high proton conductivity of 2.0×10^{-3} S/cm. Notably, these electrolytes demonstrate strong adhesion with activated carbon electrodes, resulting in flexible supercapacitors with a stable electrolyte-electrode interface that retains 90% capacitance after 14,000 charge-discharge cycles and 10,000 bending cycles. This study provides a promising approach for developing nanocluster-based soft electrolyte materials for flexible devices.

© 2026 Published by Elsevier B.V. on behalf of Chinese Chemical Society and Institute of Materia Medica, Chinese Academy of Medical Sciences.

Proton conductors play crucial roles in energy and electronic technologies, serving as essential electrolyte materials in various energy conversion and storage devices, including fuel cells, supercapacitors, and water electrolysis systems [1–6]. To ensure the stable operation of these devices, proton conductors need to possess several fundamental properties: high ionic conductivity, robust mechanical stability, strong interfacial adhesion, and ease of processing [7–10]. Polyoxometalates (POMs), nanoscale metal oxide clusters typically around 1 nm, are excellent inorganic proton conductors [11–17]. The delocalized negative charges on POM cluster skeletons facilitate the easy dissociation of protons from their surface, imparting POMs with super-acidity. However, the proton conductivity of POMs significantly decreases in low humidity conditions, limiting their practical applications [18–23]. Moreover, POMs are usually crystalline and brittle powders, lacking the necessary processability to assemble electrochemical devices [24–27]. These limitations impede the development of POM-based proton conductors. Therefore, it is crucial to develop innovative POM-based electrolytes that exhibit both high conductivity and desirable mechanical properties, ease of processing, and strong interfacial adhesion with electrodes.

By employing an organic-inorganic composite strategy, inorganic colloidal nanomaterials can be integrated into organic and polymer soft matrices [28–32]. This approach effectively combines the functional properties of inorganic components with the excellent processability of organic components, resulting in composite materials with superior comprehensive performance. This strategy is also widely employed in the development of high-performance electrolyte materials. For POMs, dispersing them into an organic soft matrix is an effective way to enhance their processability. In the reported works, Yin *et al.* combined low molecular weight polyethylene glycol with POMs through hydrogen bonding networks to create pseudo-plastic fluidic nanocomposites [33,34]. These materials exhibit exceptional proton conductivity but have relatively low mechanical strength. Besides, Zang *et al.* introduced POMs into polymer gel networks using a one-pot crosslinking method, resulting in ionic hydrogels with good mechanical properties [35,36]. However, due to the intrinsic need for solvents to facilitate ion transport in gel materials, there is an unavoidable risk of solvent evaporation. Therefore, constructing a POM-accommodating matrix network that combines the fluidity of small molecules with the mechanical strength and non-volatility of polymers is particularly important.

In this work, we have successfully developed a POM-based flexible and processable electrolyte that combines polymer-like mechanical characteristics with high proton conductivity by incorporating POM nanoclusters into a supramolecular ionic network (SIN) (Fig. 1). POMs are dispersed into bola-type zwitterionic liquids through electrostatic and hydrogen bonding interactions, forming

* Corresponding authors.
E-mail addresses: chaisc@mail.jlu.edu.cn (S. Chai), hl_li@jlu.edu.cn (H. Li).

https://doi.org/10.1016/j.cclet.2024.110750
1001-8417/© 2026 Published by Elsevier B.V. on behalf of Chinese Chemical Society and Institute of Materia Medica, Chinese Academy of Medical Sciences.

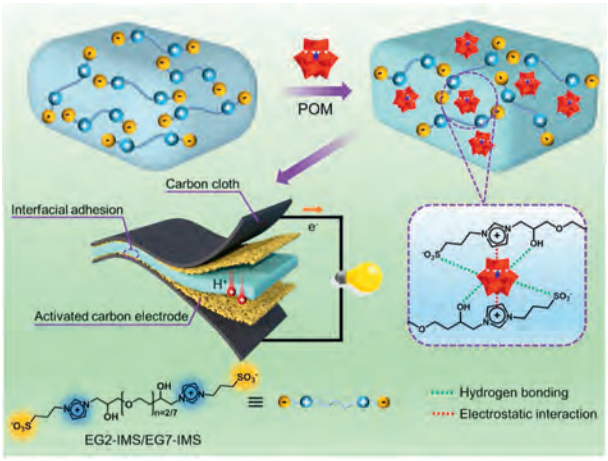


Fig. 1. Schematic illustration of the preparation of SIN electrolytes and fabrication of supercapacitors.

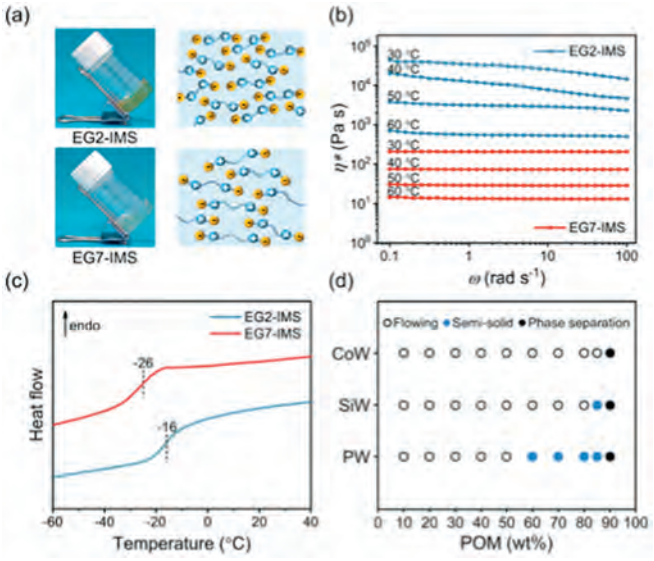


Fig. 2. (a) Photographs and schematic illustration of two zwitterionic liquids. (b) Viscosities versus shearing rates at different temperatures. (c) Glass transition temperature of two zwitterionic liquids. (d) The phase diagram of EG2-IMS composited with three POMs of different charge numbers.

an ionic network structure. Serving as the nodes of this network, the protons on the POM surface can be transported *via* hopping during the network dynamic reorganization [17,37–39]. The resulting SIN electrolytes exhibit the unique dynamic reversibility of supramolecular polymers, with non-covalent interactions imparting thermal and shear responsiveness, while also demonstrating excellent interfacial adhesion. We have successfully applied this material as a flexible, adhesive proton conductor in flexible supercapacitors. This work not only provides a new strategy for preparing POM-based soft materials but also highlights the significant potential of SIN electrolyte materials in the field of flexible energy and electronic devices.

Two bola-type zwitterionic liquids were synthesized with polyethylene glycol oligomer spacer and imidazole sulfonate zwitterion terminal. The synthesis method and characterization are detailed in Supporting information (Figs. S1-S3 in Supporting information). Imidazole rings can interact with POM anions through electrostatic interaction, which is the predominant driving force for forming the SINs. Meanwhile, the sulfonate groups can accept protons from POMs and form a dense hydrogen bond network with the closely packed oxygen atoms on the POM surface, providing a continuous pathway for proton hopping [40]. To compare the effects of flexible spacers, we selected two polyethylene glycol oligomers with 2 and 7 ethylene glycol (EG) repeat units and named the corresponding zwitterionic liquid molecules EG2-IMS and EG7-IMS. By combining these two zwitterionic liquids with Keggin-type POMs that possess different charges and proton numbers, we developed flexible, self-supporting SIN materials.

Imidazole-sulfonate zwitterions are typical crystalline compounds, usually appearing as solid powders [41]. Incorporating flexible EG units into their structure inhibited zwitterion crystallization, resulting in fluid bola-type zwitterionic liquids (Fig. 2a). Rheological tests show that EG2-IMS and EG7-IMS are viscous liquids, with zero-shear viscosities at 30 °C of 4.5×10^4 and 2.1×10^2 Pa s, respectively, the former being two orders of magnitude higher than the latter (Fig. 2b). EG7-IMS maintains stable viscosity at shear rates, while EG2-IMS exhibits shear thinning at room temperature. This indicates that a shorter spacer leads to a higher ionic group density and stronger intermolecular electrostatic interactions, facilitating a polymer-like SIN structure [42–44]. When temperature exceeds 60 °C, the accelerated molecular movement balances the dissociation and recombination of these electrostatic interactions, leading to a stable viscosity. Differential scanning calorimetry (DSC) and thermogravimetric analysis (TGA) were used to analyze the thermal phase behavior and decomposition temperature of the zwitterionic liquids. Fig. 2c and Fig. S4 (Supporting information) show T_g of −16 °C and −26 °C, respectively. The EG2-IMS system exhibits higher T_g and decomposition temperature, suggesting that a shorter PEG spacer enhances thermal stability.

POMs are proton-rich ionic inorganic nanoclusters, act as electrostatic cross-linkers and proton conductors by dissociating into multi-charged anions and free protons in polar media. To study the effect of POMs with varying proton counts on the SIN structure, three Keggin-type POMs, $H_3PW_{12}O_{40}$ (PW), $H_4SiW_{12}O_{40}$ (SiW), and $H_6CoW_{12}O_{40}$ (CoW) were selected as representatives. All three POMs have the same size but contain 3, 4, and 6 protons, respectively. Synthesis and Fourier transform infrared (FT-IR) data are shown in Fig. S5 (Supporting information). Since three POMs are soluble in both zwitterionic liquids, we prepared SIN electrolytes by directly blending POMs into the zwitterionic liquids (Tables S1 and S2 in Supporting information). The composite samples are named EG2-IMS/POMX or EG7-IMS/POMX, where X denotes the weight percentage of POMs.

The state diagram of composite samples with different POM contents is shown in Fig. 2d. With increasing the POM content, zwitterionic liquids are gradually solidified with increased viscosities; eventually, macroscopic phase separation occurs when POM content exceeds 85 wt%. Notably, homogeneous samples with high POM content exhibit flexible semi-solid regions. When PW content in EG2-IMS is 60 wt% to 85 wt%, the sample behaves as a homogeneous semi-solid material. As the charge number of POMs increases, the semi-solid phase region narrows. SiW can form a semi-solid sample with EG2-IMS at around 85 wt%, while CoW cannot form a semi-solid sample with EG2-IMS, remaining in a fluid state even at 85 wt% POM content. The phase diagram of EG7-IMS and POM composite systems is similar to that of EG2-IMS (Fig. S6 in Supporting information). These results indicate that the increasing number of protons on POMs is not beneficial to form SIN with zwitterionic liquids. We speculate this is because the free protons dissociated from POMs neutralize the negative charges of sulfonate groups, weakening the electrostatic interaction between sulfonate groups and imidazole cations of adjacent zwitterionic liquid molecules, thereby reducing the strength of the SIN to realize solidification. Consequently, PW and SiW, due to the appropri-

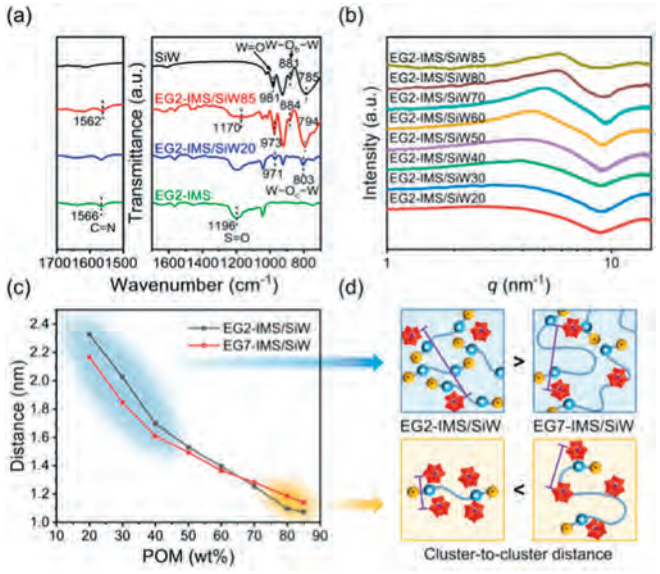


Fig. 3. (a) FT-IR spectra of SiW, EG2-IMS, EG2-IMS/SiW20, and EG2-IMS/SiW85. (b) SAXS data of SINs composed of different contents of SiW and EG2-IMS. (c) Cluster-to-cluster distances of SiW in EG2-SiW calculated from the SAXS data and (d) the schematics of cluster-to-cluster distances.

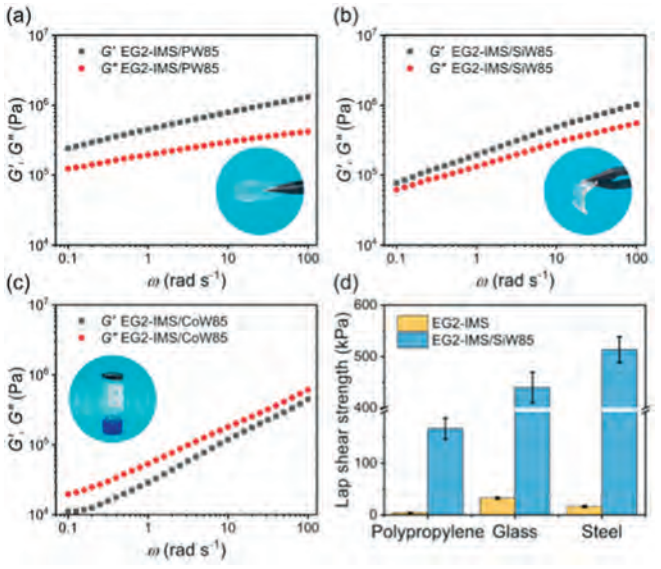


Fig. 4. Storage modulus (G') and loss modulus (G'') of (a) EG2-IMS/PW85, (b) EG2-IMS/SiW85 and (c) EG2-IMS/CoW85 *versus* shearing rates at 30 °C. Insets are the photographs of these samples. (d) Lap shear strengths of EG2-IMS/SiW85 on polypropylene, glass, and stainless-steel substrates.

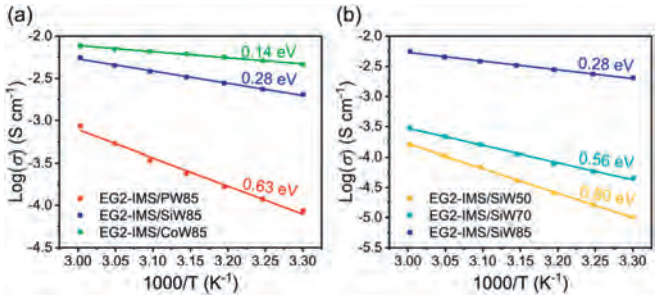


Fig. 5. Temperature-dependent proton conductivities of (a) EG2-IMS/PW85, EG2-IMS/SiW85 and EG2-IMS/CoW85, (b) EG2-IMS/SiW composite samples with varied SiW contents of 50, 70, and 85 wt%.

ate number of protons, are suitable for preparing semi-solid POM-based SIN electrolytes.

The high solubility of POMs in zwitterionic liquids is due to their intermolecular interactions. Taking the SiW and EG2-IMS composite system as an example, FT-IR spectra show that the characteristic vibrational peaks of $W{-}O_b{-}W$ and $W{-}O_c{-}W$ attributed to SiW in EG2-IMS/SiW20 and EG2-IMS/SiW85 occur blue shifts compared to pure SiW, reflecting changes in the electrostatic environment surrounding SiW (Fig. 3a). Meanwhile, from EG2-IMS to EG2-IMS/SiW85, the S=O vibration shows a red shift from 1196 cm^{-1} to 1170 cm^{-1}, indicating hydrogen bonding between sulfonate groups and the protons on the surface of SiW. Additionally, the C=N vibrational peak red-shifts from 1566 cm^{-1} to 1562 cm^{-1}, indicating electrostatic interactions between the cationic imidazole group and the anionic SiW clusters [40].

The distribution of POM in the zwitterionic matrix was studied by small angle X-ray scattering (SAXS) and X-ray diffraction (XRD), using EG2-SiW as an example (Fig. 3b). The scattering peaks can reflect the average spacing between SiW nanoclusters [45]. As SiW content rises, the scattering peaks shift to a high-q region, indicating that the spacing between SiW decreases. From 20 wt% to 85 wt% SiW, spacing in EG2-IMS matrix decreases from 2.33 nm to 1.07 nm, and in EG7-IMS from 2.17 nm to 1.14 nm (Fig. 3c), with EG2-IMS having smaller spacing due to the small volume causing denser packing (Fig. 3d). The phase stability of SIN electrolytes with the highest POM content, while maintaining macroscopic homogeneity, was studied using XRD. The XRD patterns of the samples, prepared over 10 days, show no crystallization peaks (Figs. S8 and S9 in Supporting information). This indicates that abundant electrostatic and hydrogen bond interactions between the zwitterionic liquids and POMs contribute to the stable dispersion of POMs in the SIN matrix.

The mechanical properties of 85 wt% POM composites in EG2-IMS/POM and EG7-IMS/POM systems were studied. In the EG2-IMS/POM system, various POMs result in distinct mechanical properties of composite samples: EG2-IMS/PW85 is a self-supporting solid, EG2-IMS/SiW85 is a flexible soft material, and EG2-IMS/CoW85 is a slow-flowing viscous liquid (Figs. 4a-c). Rheological tests reveal that EG2-IMS/PW85 has a much higher storage modulus (G') than loss modulus (G''), showing solid-like behavior. EG2-IMS/SiW85 has a G' value higher than G'', but the modulus values are low and similar, indicating a semi-solid state. In contrast, EG2-IMS/CoW85 exhibits a G'' value higher than G', which is characteristic of liquid state. At 1 rad/s, G' values for EG2-IMS/PW85, EG2-IMS/SiW85, and EG2-IMS/CoW85 were 4.5×10^5, 1.9×10^5, and 2.9×10^4 Pa, respectively. Additionally, all samples displayed shear thinning (Fig. S10 in Supporting information), suggesting that at high shear rates, the SIN network disrupted, decreasing sample viscosity and confirming internal network structures. The modulus and viscosity of EG7-IMS/POM follow trends like EG2-IMS/POM but with lower modulus values (Fig. S11 in Supporting information).

The polarity and charge characteristics of POMs and zwitterions in SIN electrolytes facilitate strong supramolecular interactions with different substrates, contributing to excellent interfacial adhesion. Additionally, the supramolecular network further enhances the cohesion of SIN electrolytes. The adhesion strength of EG2-IMS/SiW85 on polypropylene, glass, and stainless steel is 166, 439, and 512 kPa, respectively, displaying adhesive properties similar to some POM-containing covalent polymer gel materials (Fig. 4d) [46].

Proton conductivity of SIN electrolytes at 30 % RH from 30 °C to 60 °C was measured by AC electrochemical impedance spectroscopy (EIS) (Fig. 5 and Table 1, Fig. S12 and Table S3 in Supporting information). The effects of proton numbers and POMs content on proton conductivity were studied. At 30 °C, EG2-IMS/PW85,

Table 1
The mechanical parameters and conductivity of SINs.[a]

Sample	T_g (°C)	G' (Pa)	G'' (Pa)	η^* (Pa s)	σ (S/cm)	E_a (eV)
EG2-PW85	16	4.5×10^5	1.9×10^5	4.9×10^5	8.6×10^{-5}	0.63
EG2-SiW85	-4	1.9×10^5	1.3×10^5	2.4×10^5	2.0×10^{-3}	0.28
EG2-CoW85	-9	2.9×10^4	5.3×10^4	0.6×10^5	4.7×10^{-3}	0.14
EG7-PW85	-8	1.4×10^5	7.5×10^4	1.6×10^5	5.8×10^{-5}	0.59
EG7-SiW85	-14	1.9×10^4	3.7×10^4	6.2×10^4	6.6×10^{-4}	0.45
EG7-CoW85	-16	2.8×10^3	4.6×10^3	5.3×10^3	1.6×10^{-3}	0.41

[a] The data listed in the table are tested at 30 °C. The storage modulus, loss modulus and viscosity are measured at 1 rad/s.

EG2-IMS/SiW85, and EG2-IMS/CoW85 showed conductivities of 5.8×10^{-5}, 2.0×10^{-3}, and 4.6×10^{-3} S/cm, respectively, suggesting a positive correlation between proton concentration and conductivity in SINs (Fig. 5a). At the same temperature, EG2-IMS/PW85 exhibited the lowest conductivity, while EG2-IMS/CoW85 showed the highest. EG7-IMS/POM samples followed a similar trend with POM changes (Fig. S12a). However, due to the larger molecular weight of EG7-IMS, which hinders molecular motion dynamics, its proton conductivity was lower than that of EG2-IMS/POM when the POM type and content remained constant. Additionally, using EG2-IMS/SiW and EG7-IMS/SiW as examples, we evaluated the impact of varying SiW content on proton conduction. A higher SiW content resulted in a higher proton conductivity (Fig. 5b and Fig. S12b). As the POM content in the system increases, the spacing between POM nanoclusters decreases, resulting in a more continuous and compact hydrogen bond network between POMs and zwitterionic liquids, thereby enhancing their synergistic conduction effect. Samples containing 85 wt% SiW exhibited the highest conductivity.

As the temperature increased, all samples displayed increased proton conductivity with Arrhenius behavior, allowing for determining activation energy (E_a) for conduction. E_a can reflect the proton conduction mechanism. Generally, E_a below 0.4 eV implies Grotthuss hopping *via* continuous hydrogen bond networks that facilitate proton hopping [47], while a value above 0.5 eV suggests proton carrier diffusion as the predominant transport process. In our study, the E_a values for EG2-IMS/PW85, EG2-IMS/SiW85, and EG2-IMS/CoW85 were 0.63, 0.28, and 0.14 eV, respectively, indicating a transition in the proton transport mechanism from diffusion-dominated to hopping-dominated, corresponding to increased connectivity of the hydrogen bonding network (Table 1). Conversely, E_a values for EG7-IMS/PW85, EG7-IMS/SiW85, and EG7-IMS/CoW85 (0.59, 0.45, and 0.41 eV) were higher than those of EG2-IMS systems, illustrating a weaker hydrogen bonding network formation.

For efficient and stable electrochemical device operation, a robust electrode-electrolyte interface and high conductivity are crucial. EG2-IMS/SiW85, with its flexibility, strong adhesion, and high proton conductivity, is ideal for electrolyte materials. To further enhance its mechanical strength, we composite it with porous nonwoven fabrics, creating a composite electrolyte membrane that integrates rigidity and flexibility (Fig. S13 in Supporting information). We integrated the composite electrolyte membrane with activated carbon electrodes to create the flexible supercapacitor SC-EG2-SiW85 and evaluated its electrochemical performance. GCD can reflect the energy efficiency and power performance of supercapacitors. GCD curves in Fig. 6a, at various current densities, are symmetric and linear, confirming double-layer capacitance. The specific capacitance calculated from GCD data is 154 mF/cm^2 at 0.5 mA/cm^2 (Fig. S14 in Supporting information). Fig. 6b reveals the stability of the specific capacitance and coulomb efficiency of SC-EG2-SiW85 during the charge-discharge cycle. After 14,000 cycles, the capacitor maintains 100% efficiency and more than 90% capacity, showing excellent electrochemical reversibility. Bending tests show the capacity retention rate decreases initially but then

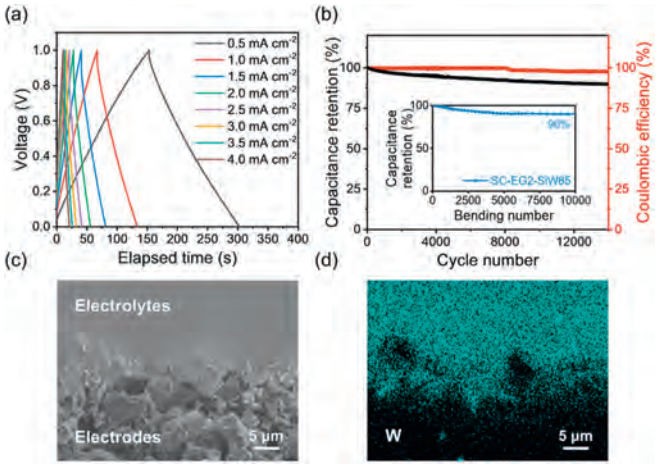


Fig. 6. (a) Galvanostatic charge-discharge (GCD) curves at different current densities. (b) Capacitance retention after 14000 cycles and capacitance retention at different bending numbers. (c) Scanning electron microscope (SEM) image and (d) energy-dispersive X-ray spectroscopy (EDX) elemental mappings of the electrode-electrolyte (EG2-IMS/SiW85) interface in the supercapacitor.

stabilizes, remaining above 90% even after 10,000 bends, proving the robust bendability of the SIN electrolyte. SEM image and EDX mapping (Figs. 6c and d) reveal the morphology of the electrode-electrolyte interface. Unlike traditional rigid materials, the flexible electrolyte can penetrate the gaps inside the electrode and closely adhere to the electrode material, thereby increasing the contact area between the electrode and electrolyte and improving interface stability [48].

In conclusion, we present the development of SIN electrolytes created by crosslinking zwitterionic liquids with POM nanoclusters. Through the synergistic effects of hydrogen bonding and electrostatic interactions, the SIN electrolytes can incorporate a high POM loading of up to 85 wt% while still maintaining semi-solid flexibility. Within the SINs, POMs not only function as crosslinking sites but also serve as proton carriers, providing free protons and creating proton transport pathways, which enables the SIN electrolytes to show a high proton conductivity of 2.0×10^{-3} S/cm at room temperature. Furthermore, the tight adhesion between the SIN electrolytes and electrodes allows their supercapacitors to achieve high capacitance, excellent stability, and certain bending resistance. After 14000 charge-discharge cycles and 10,000 bends, the capacitance retention remains over 90%. This work innovatively integrates POM nanoclusters into SIN matrices, providing a new approach to the development of nanocluster-based soft electrolyte materials. With the tunable structures of POMs and organic substrates, these electrolytes have substantial potential for functional expansion and applications in the energy and electronics fields.

Declaration of competing interest

The authors declare that they have no known competing financial interests or personal relationships that could have appeared to influence the work reported in this paper.

CRediT authorship contribution statement

Xiang Li: Writing – original draft, Project administration, Methodology, Investigation, Formal analysis, Data curation. **Haikun Guo:** Formal analysis. **Shengchao Chai:** Methodology. **Haibin Li:** Methodology. **Shihao Song:** Data curation. **Peng Zuo:** Validation. **Haolong Li:** Writing – review & editing, Supervision, Funding acquisition, Formal analysis.

Acknowledgments

The authors gratefully acknowledge the support from the National Natural Science Foundation of China (Nos. 92261110, 22075097) and the education department of Jilin province (No. JJKH20241248CY).

Supplementary materials

Supplementary material associated with this article can be found, in the online version, at doi:10.1016/j.cclet.2024.110750.

References

[1] C. Laberty-Robert, K. Vallé, F. Pereira, et al., Chem. Soc. Rev. 40 (2011) 961–1005.
[2] C. Klose, T. Saatkamp, A. Münchinger, et al., Adv. Energy Mater. 10 (2020) 1903995.
[3] X. Fan, C. Zhong, J. Liu, et al., Chem. Rev. 122 (2022) 17155–17239.
[4] C.S. Gittleman, H. Jia, E.S. De Castro, et al., Joule 5 (2021) 1660–1677.
[5] Y. Liu, B. Tian, F. Ning, et al., Adv. Energy Mater. 14 (2024) 2303353.
[6] R. Haider, Y. Wen, Z.F. Ma, et al., Chem. Soc. Rev. 50 (2021) 1138–1187.
[7] Y. Liang, F. Zhao, Z. Cheng, et al., Energy Environ. Sci. 11 (2018) 1730–1735.
[8] H. Guo, M. Zeng, X. Li, et al., ACS Appl. Mater. Interfaces 13 (2021) 30039–30050.
[9] G. Wang, C. Chen, Y. Chen, et al., Angew. Chem. Int. Ed. 59 (2020) 2055–2060.
[10] M. Zhang, R. Yu, X. Tao, et al., Adv. Funct. Mater. 33 (2023) 2208083.
[11] D.E. Katsoulis, Chem. Rev. 98 (1998) 359–388.
[12] L. Zhai, H. Li, Molecules 24 (2019) 3425–3444.
[13] G. Wang, J. Li, L. Shang, et al., CCS Chem. 4 (2022) 151–161.
[14] J.H. Kruse, M. Langer, I. Romanenko, et al., Adv. Funct. Mater. 32 (2022) 2208428.
[15] R.L. Liu, Y. Chen, X. Su, et al., Coord. Chem. Rev. 522 (2025) 216224.
[16] H. Guo, L. Li, X. Xu, et al., Angew. Chem. Int. Ed. 61 (2022) e202210695.
[17] X. Li, S. Chai, L. Zhai, et al., Macromol. Rapid Commun. 44 (2023) 2300223.
[18] N. Ogiwara, T. Iwano, T. Ito, et al., Coord. Chem. Rev. 462 (2022) 214524.
[19] X. Li, S. Chai, H. Li, Dalton Trans. 53 (2024) 6488–6495.
[20] S. Chai, R. Zhong, L. Zhai, et al., Fundam. Res. (2023), doi:10.1016/j.fmre.2023.09.003.
[21] H. He, Y. Zhu, T. Li, et al., ACS Nano 16 (2022) 19240–19252.
[22] H. He, G. Wang, S. Chai, et al., Chin. Chem. Lett. 32 (2021) 2013–2016.
[23] A. Wu, X. Gao, P. Sun, et al., Angew. Chem. Int. Ed. 57 (2018) 4025–4029.
[24] A. Martinelli, J.M. Otero-Mato, M.N. Garaga, et al., J. Am. Chem. Soc. 143 (2021) 13895–13907.
[25] X.M. Li, Y. Wang, Y. Mu, et al., ACS Appl. Mater. Interfaces 14 (2022) 9264–9271.
[26] S. Li, Y. Zhao, S. Knoll, et al., Angew. Chem. Int. Ed. 60 (2021) 16953–16957.
[27] J. Luo, X. Sun, J.F. Yin, et al., Giant 2 (2020) 100013.
[28] R. Gangopadhyay, A. De, Chem. Mater. 12 (2000) 608–622.
[29] L. Zhai, Y.L. Zhu, G. Wang, et al., Nano Lett. 23 (2023) 3887–3896.
[30] Q. Zhang, L. He, H. Wang, et al., Chem. Commun. 48 (2012) 7067–7069.
[31] W. Wang, T. Liu, T. Zhao, et al., Adv. Sci. 11 (2024) 2305102.
[32] X. Pu, Q. Cao, X. He, et al., Adv. Energy Mater. 14 (2024) 2303972.
[33] Z. Zheng, Q. Zhou, M. Li, et al., Chem. Sci. 10 (2019) 7333–7339.
[34] Z. Zheng, M. Li, Y. Lai, et al., Macromol. Rapid Commun. 44 (2023) 2200227.
[35] D. Cheng, B. Li, S. Sun, et al., CCS Chem. 2 (2020) 1649–1658.
[36] Z.D. Wang, K. Bo, C.L. Zhong, et al., Adv. Mater. 36 (2024) 2400099.
[37] H. Huang, Y. Fang, Y. Weng, et al., Mater. Today Chem. 32 (2023) 101670.
[38] H. Qiao, B. Wu, S. Sun, et al., J. Am. Chem. Soc. 146 (2024) 7533–7542.
[39] W. Li, H. Zhang, W. Lu, et al., Adv. Optical Mater. 11 (2023) 2202738.
[40] S. Chai, F. Xu, R. Zhang, et al., J. Am. Chem. Soc. 143 (2021) 21433–21442.
[41] M. Yoshizawa, M. Hirao, K. Ito-Akita, H. Ohno, J. Mater. Chem. 11 (2001) 1057–1062.
[42] M.A. Aboudzadeh, M.Eugenia Munoz, A. Santamaria, et al., Macromol. Rapid Commun. 33 (2012) 314–318.
[43] A. Aboudzadeh, M. Fernandez, M.E. Muñoz, et al., Macromol. Rapid Commun. 35 (2014) 460–465.
[44] M. Wathier, M.W. Grinstaff, J. Am. Chem. Soc. 130 (2008) 9648–9649.
[45] L. Liu, A. Huang, J. Yang, et al., Angew. Chem. Int. Ed. 63 (2024) e202318355.
[46] Q. Yu, Z. Zheng, X. Dong, et al., Soft Matter 17 (2021) 8786–8804.
[47] A. Shigematsu, T. Yamada, H. Kitagawa, J. Am. Chem. Soc. 133 (2011) 2034–2036.
[48] X. Li, J. Shao, S.K. Kim, et al., Nat. Commun. 9 (2018) 2578.